LONDON'S GLOBAL UNIVERSITY

UCL

7,498 words/25 pages

Patch-clamp Analysis of Miniature Synaptic Currents in Layer 5 Cortical Pyramidal Cells of a Bardet-Biedl Syndrome Mouse Model

Jing Xuan Lim
(S/N: 110043614)
Bsc Neuroscience

Thesis submitted for NEUR3903: Extended Experimental Project

UNIVERSITY COLLEGE LONDON

DIVISION OF BIOSCIENCES

DEPARTMENT OF NEUROSCIENCE, PHYSIOLOGY & PHARMACOLOGY

Abstract

Primary ciliopathies are known to be strongly associated with neural defects. Bardet-Biedl Syndrome (BBS) is one such disorder that counts intellectual disability as one of its defining features. How primary cilia defects lead to deficits in learning and memory, however, are largely unknown. Recent evidence suggests that disrupting ciliation in cortical neurons leads to impaired dendritic refinement and reduced synapse formation, thereby affecting proper circuit formation. BBS4 and BBS5 are BBS-associated genes that code for components of the BBSome, an intracellular structure required for ciliary biogenesis and function. Preliminary results showed a reduction in the spine density of cortical neurons of Bbs4 ($Bbs4^{-/-}$) and Bbs5 ($Bbs5^{-/-}$) knockout mice. Whether this was accompanied by a diminished synaptic function is unknown. Recording from layer 5 cortical pyramidal cells, we found that $Bbs5^{-/-}$ has no impact on the mean frequency and amplitude of miniature excitatory and inhibitory synaptic current. Interestingly, we observed a redistribution of synaptic inputs towards perisomatic sites, possibly via compensatory mechanisms. In light of these findings, we speculate that BBS5 defects in the neocortex have a reduced role in causing learning impairments in BBS patients.

Acknowledgements

I thank Dr B. Clark for technical training, for carrying out animal dissection and preparation of brain slices, and for comments on the manuscript; and Dr C. Schmidt-Hieber for help with data analysis.

Introduction

Cilia are ancient eukaryotic organelles that project from the cell surface (Tobin and Beales, 2007). They fall into one of two types: primary (non-motile) or secondary (motile), so categorized due to their readily observable differences in motility. Because of their lack of motility and their sometimes short appearance, primary cilia are thought to be vestigial for a very long time. In recent years however, the primary cilium is starting to gain recognition as a key sensory process and the root cause for a variety of human diseases. Interestingly, neurological involvement in these diseases is high, with intellectual disability a common clinical feature (Valente et al., 2014).

Primary Cilia

Primary cilia are small, immotile membrane-bound organelles that protrude out of almost all vertebrate cell types (Fig. 1*A*). These hair-like structures are normally present at a frequency of one per cell (Fig. 1*B*), and are highly conserved throughout evolution. A ring of doublet microtubule scaffolding arranged in a 9+0 formation – the axoneme – forms the core of the cilium (Fig. 1*C*,*D*). At the base of the axoneme is the basal body, a modified mother centriole, which anchors the axoneme in the cell. Between the axoneme and the basal body is the transition zone, a ciliary pore that controls the traffic of molecules entering and leaving the cilium. The function of primary cilia are manifold. They have been found to have critical roles in sensing the extracellular environment by acting as mechanoreceptors, chemoreceptors, photoreceptors, osmoreceptors, thermoreceptors, and gravity receptors (Christensen et al., 2005; Insinna and Besharse, 2008; Moorman and Shorr, 2008; Satir et al., 2010; Kuhara, 2012). A high concentration of various G-protein coupled receptors (GPCRs) are expressed on the surface of the primary cilium. These GPCRs respond to specific hormones, growth factors and morphogens (sonic hedgehog [SHH] and Wnt) (Haycraft et al., 2005; Huangfu and Anderson, 2005; Lancaster et al., 2011; Wallingford and Mitchell, 2011; Higginbotham et al., 2013). The primary cilium therefore also plays a role in coordinating developmental and homeostatic signalling pathways (Goetz and Anderson, 2010). These functions stem from the organelle's unique location (away from the soma but near to the Golgi and vesicle transport system) and structure which results in effective compartmentalisation within the cell, and its fortuitous position at the interface between the intracellular and extracellular milieu, allowing the fine tuning of specialized responses to different stimuli (Szymanska and Johnson, 2012).

Bardet-Biedl Syndrome

Given their diverse function, it is not surprising that the disruption of primary cilia can have wide-ranging consequences. Primary ciliopathies are disorders and diseases that arise as a result of defective primary cilia. BBS, a heterogeneous autosomal recessive disorder, is an example of a primary ciliopathy. At present, 18 BBS genes have been identified. They are

BBS1, BBS2, ARL6 (BBS3), BBS4, BBS5, MKKS (BBS6), BBS7, TTC8 (BBS8), PTHB1 (BBS9), BBS10, TRIM32 (BBS11), BBS12, MKS1 (BBS13), CEP290 (BBS14), WDPCP (BBS15), SDCCAG8 (BBS16), LZTFL1 (BBS17) and BBIP1 (BBS18) (Forsythe and Beales,

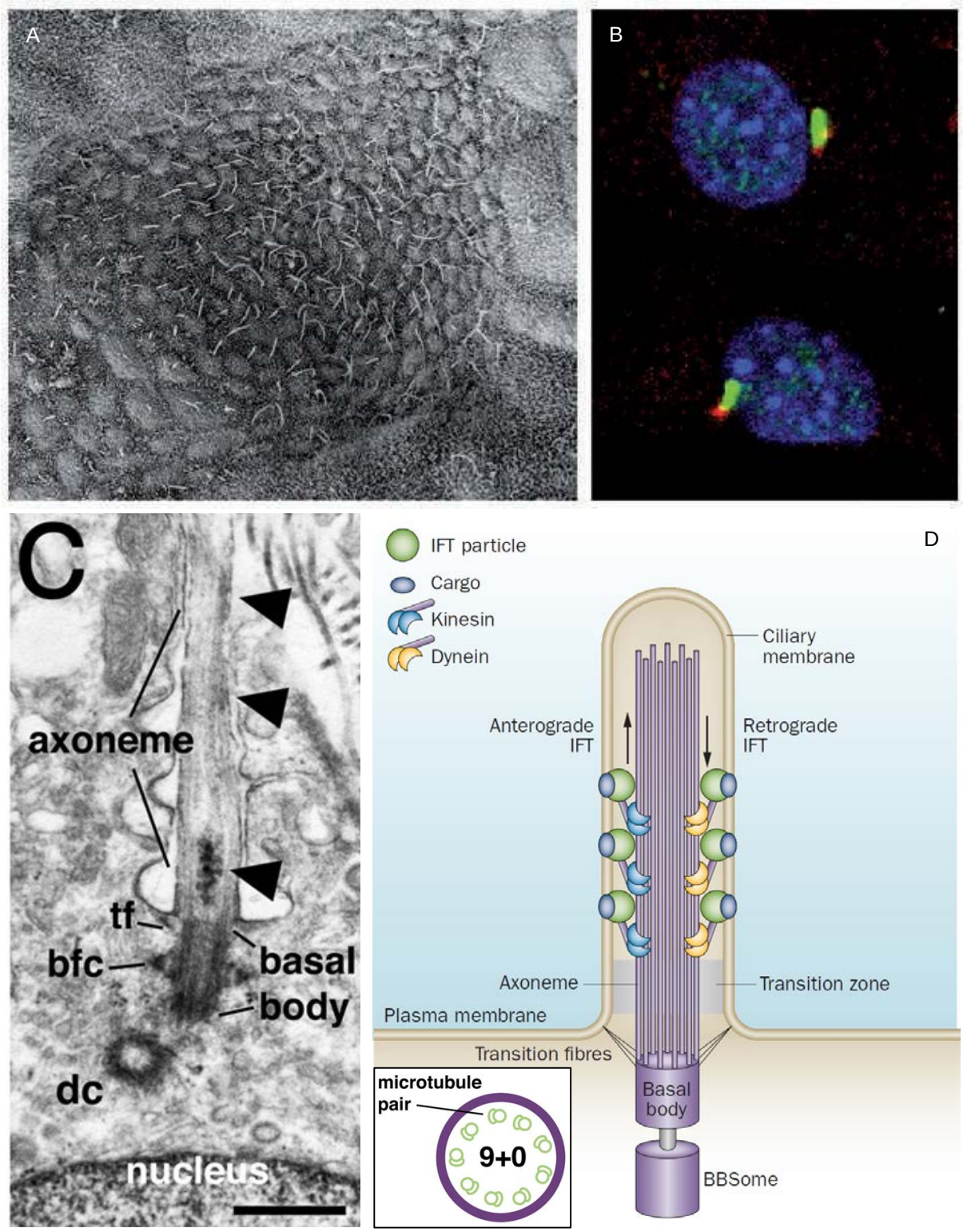

Figure 1. Structure, organisation and workings of the primary cilium. ***A,*** Electronmicrograph showing mammalian nodal cilia of the mouse embryo at embryonic day 7.75. Taken from Goetz and Anderson (2010). ***B***, Confocal image of embryonic fibroblasts stained for cilia (green), basal bodies (red) and nuclei (blue). Taken from Goetz and Anderson (2010). ***C***, Electronmicrograph of a primary cilium in an adult mouse brain. Visible

features include the axoneme, basal body, a transition fibre (tf), the basal foot and cap (bfc), and the daughter centriole (dc). Arrowheads point to possible IFT particles travelling along the cilium. Scale bar, 0.5 µm. Taken from Louvi and Grove (2011). ***D***, A schematic diagram showing the major features of the primary cilium. In addition to the exterior and visible features shown in (***C***), the interior features can also be seen. The axoneme is composed of microtubule doublets (purple tubes) arranged in a 9+0 fashion. (Inset) A cross-section through the axoneme showing the organisation of the microtubules pairs (green). Other features include the ciliary membrane, transition zone and the basal body. The BBSome is a component of the basal body that contains proteins that are implicated in BBS, hence its name. The function of the individual proteins are still unclear. Protein cargo is transported up and down the cilium via the IFT machinery. Anterograde trafficking is mediated by IFT B and kinesin motor proteins (blue) while retrograde trafficking is mediated by IFT A and dynein motor proteins (yellow). Taken from Valente et al. (2014) and Louvi and Grove (2011).

2014). These genes are responsible for encoding components of the BBSome (Fig. 1*D*), a component of the basal body that is important for the assembly, functioning and regulation of the intraflagellar transport (IFT) machinery (Ansley et al., 2003). IFT function is essential for ciliary biogenesis and signalling.

BBS is pleiotropic – a single mutated gene can have effects on multiple, seemingly unrelated phenotypic traits across major body systems. Symptoms of BBS patients can include age-related retinal dystrophy, early-onset obesity, postaxial polydactyly, renal dysplasia, genitourinary tract abnormalities, subclinical hearing loss, and various neurological impairments such as mild-to-moderate cognitive impairment, delayed motor developmental milestones and speech acquisition, ataxia and poor motor coordination, hydrocephalus, and reduced hippocampal volume (Forsythe and Beales, 2012). Given its wide-ranging neurological consequences, and in particular implications for learning and memory, we were interested in the effects of BBS malfunction on cortical synaptogenesis.

Synaptogenesis

The formation of functional neural connections is a dynamic process that occurs in the developing brain and persists well into adulthood. This process is thought to underlie learning and memory. Synaptogenesis involves a signalling cascade comprising of “priming” events such as axonal guidance, dendritic morphogenesis, target recognition, and stabilization of early contact sites; “inducing” pre- and post-synaptic differentiation and assembly events; and finally, synaptic maturation, which involves an expansion in synapse size and dendritic spine morphogenesis (Fig. 2) (Waites et al., 2005). Even when synapse formation is complete, synapses can still be subjected to activity-dependent modifications (Waites et al., 2005). Pruning of inappropriate or ineffective synapses is thought to be crucial for the fine-tuning of neuronal networks.

There is a growing body of evidence that suggests that disrupting primary cilia structure or function produces abnormal dendritic morphology in cortical areas, which might in turn

adversely affect the proper integration of defective neurons into functional circuits, thereby implicating cognitive function (Fig. 3*A*). Conditional deletion of primary cilia from new-born hippocampal dentate granule cells (DGCs) leads to defects in dendritic refinement and the proper establishment of functional synapses (Kumamoto et al., 2012). In developing neocortical neurons, both the acceleration and blocking of ciliogenesis led to a reduction in the complexity of the dendritic arbours (Guadiana et al., 2013). However, it is not known whether a less complex dendritic morphology is accompanied by a change in synapse number or strength. Preliminary experiments in Bbs knockout mice show a significant reduction in overall spine density of layer 5 cortical pyramidal cells and DGCs in Bbs4$^{-/-}$, and a smaller but significant reduction in overall spine density of DGCs in Bbs5$^{-/-}$ mice (Fig. 3*B*, figure courtesy of S. Christou-Savina and P. Beales, Institute of Child Health, London).

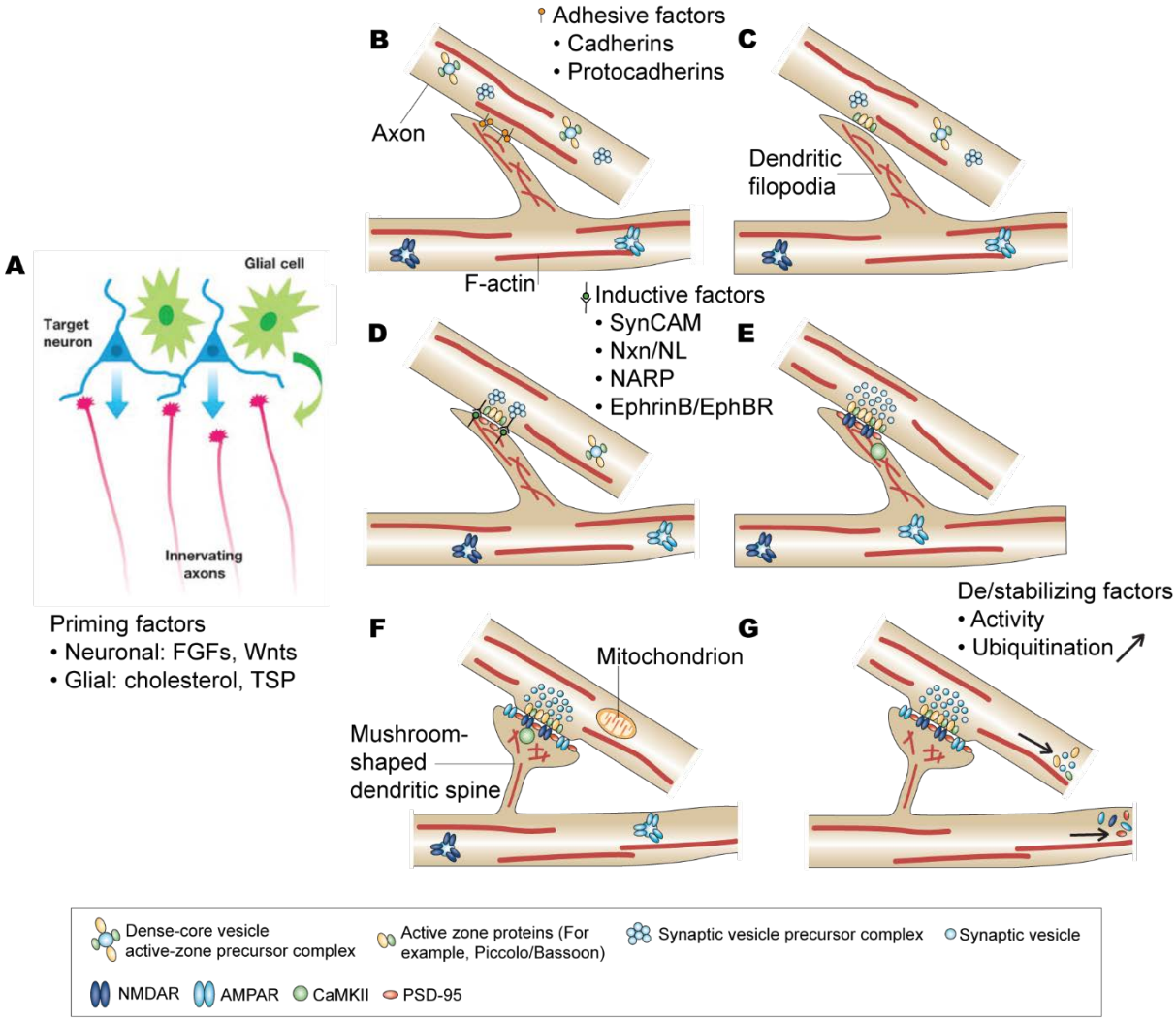

Figure 2. The temporal sequence of the molecular control of synaptogenesis. Synaptogenesis is a multistep process that can be broken down into three main steps: target contact and recognition, synapse assembly, and synaptic maturation, which is characterised by the formation of mushroom-like spines. (***A***) – (***G***) walks through this process in more detail, showing also the morphological changes that occur. ***A***, Prior to synapse formation, axons are guided to their targets by molecules such as netrins and semaphorins. At the

same time, dendritic filopodia display seeking behaviour. Priming factors secreted by target neurons and surrounding glia such as fibroblast growth factors (FGFs), Wnts, cholesterol, and thrombospondin (TSP) act to promote axonal and dendritic maturation and initiate synaptogenesis. ***B***, Adhesive factors such as cadherins and protocadherins determine the receptive field of synapse formation and thus promote specific contact. ***C***, Active zone proteins such as Piccolo and Bassoon rapidly congregate at presynaptic sites. ***D***, Inductive factors such as SynCAM and Neuroligin (NL) induce the formation of the presynaptic active zone, which becomes neurotransmitter release-competent shortly after. Postsynaptic-density protein of 95 kDa (PSD-95) accumulates at postsynaptic sites. ***E***, NL-binding partner *β*-neurexin (Nxn), Narp and Ephrin B promote the recruitment of glutamate receptors. NMDARs are recruited to the postsynaptic membrane. ***F***, AMPARs are recruited after NMDARs. This coincides with formation of spines, mushroom-like protrusions with a well-defined head, and the activation of Ca^{2+}/calmodulin-dependent protein kinase II (CaMKII). ***G***, Neuronal activity or the lack thereof stabilizes or destabilizes the synapse respectively. The latter might lead to the eventual elimination of the synapse. Ubiquitination-mediated degradation is activity-dependent, and results in synapse elimination. Figure (***A***) taken from Waites et al. (2005). Figures (***B***) – (***G***) are adapted from Li and Sheng (2003).

Given the evidence for structural changes in the neocortex of a BBS disease model, we therefore asked whether neuronal integration into functional circuits is affected in $Bbs5^{-/-}$ mice. To test neuronal connectivity, we recorded miniature synaptic currents (mPSCs) in layer 5 pyramidal cells in acute cortical slices. We hypothesized that we would detect a reduced miniature excitatory postsynaptic current (mEPSC) frequency should there be a reduction in neocortical spine density, in agreement with the structural changes we saw in the other models discussed above. We find instead no difference in mEPSC and miniature inhibitory postsynaptic current (mIPSC) frequency, suggesting that the $Bbs5^{-/-}$ cells were able to form normal levels of functional synapses. We additionally found no difference in mean mEPSC and mIPSC amplitude, although their distributions were significantly shifted towards greater amplitudes.

Materials and Methods

Slice preparation. $Bbs5^{-/-}$ ($Bbs5^{tm1b(EUCOMM)Wtsi}$/H genetic background) (Fig. 3*C*) and control (wild type litter mates, C57BL/6NTac- genetic background) mice were housed under identical standard conditions and processed at postnatal day 30 (P30)-P40 for electrophysiological recordings. Mice were decapitated under isoflurane anaesthesia and the brain was removed in ice-cold slicing artificial cerebrospinal fluid (ACSF) solution. Slicing ACSF contained the following (in mM): 120 NaCl, 2.5 KCl, 26 $NaHCO_3$, 1.5 NaH_2PO_4, 25 glucose, 0.5 $CaCl_2$ and 4 $MgCl_2$, and was bubbled with 5% carbon dioxide, 95% oxygen (henceforth referred to as carbogen). The brain was placed in a Petri dish filled with ice-cold, carbogenated slicing ACSF, the cerebellum removed and a coronal cut was made to remove approximately 3 mm of anterior neocortex. The tissue block was then glued on the anterior cut surface, dorsal surface facing the slicing blade, onto a cooled slicing stage of a vibrating microtome (Leica VT1200S). Coronal slices (250 µm) were cut from somatosensory and motor cortical regions and

transferred to an incubation chamber filled with carbogenated recording ACSF at 34°C. Recording ACSF contained the following (in mM): 120 NaCl, 2.5 KCl, 26 $NaHCO_3$, 1.5

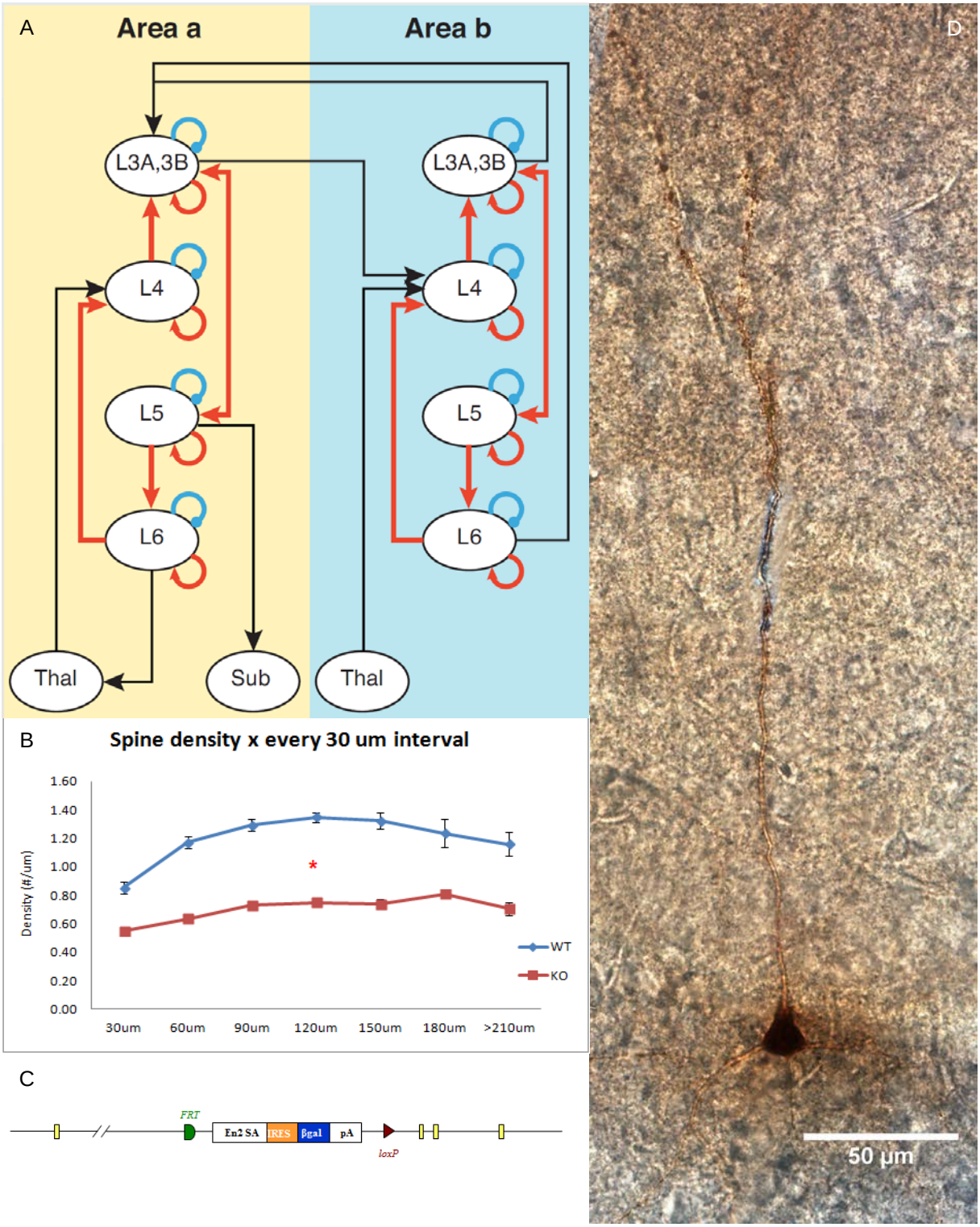

Figure 3. Bbs5$^{-/-}$ in the neocortex. ***A***, canonical microcircuits in the cortex. Red arrows represent feedforward connections, blue arrow represent feedback connections, and black arrows represent long-distance inputs. Taken from Markov et al. (2013). ***B***, Comparison of spine density of wild type and Bbs4$^{-/-}$ layer 5 cortical pyramidal cells at every 30 µm interval from the soma (*p<0.05, ANOVA and post-hoc tests). Figure courtesy of S. Christou-Savina, P. Beales, Institute of Child Health, London. ***C***, Bbs5$^{-/-}$ with the Tm1b allele. ***D***, Biocytin-stained layer-5 cortical pyramidal cell.

NaH_2PO_4, 25 glucose, 2 $CaCl_2$ and 1 $MgCl_2$ (pH7.4, when bubbled with carbogen). The slices were left in the incubation chamber at 34°C for 30-60 minutes and kept at room temperature (20°C) until use. All procedures were carried out under licence from the Home Office and were approved by local ethical review (UCL AWERB).

Electrophysiology. A brain slice was transferred to the recording chamber and is secured by a 'harp', a piece of horseshoe-shaped platinum with parallel nylon threads strung across. The recording chamber is continually superfused with carbogenated recording ACSF enriched with the following drugs (in μM): 0.5 tetrodotoxin (TTX) to block action potential initiation, and either 20 SR-95531 (Tocris) or 3000 kynurenic acid (Sigma-Aldrich) to block γ-aminobutyric acid A receptor ($GABA_AR$) or α-amino-3-hydroxy-5-methyl-4-isoxazolepropionic acid receptor (AMPAR), *N*-methyl-$_D$-aspartate receptor (NMDAR) and Kainate receptor function respectively, and was thermoregulated at 32-34°C. Whole-cell patch-clamp recordings (Hamill et al., 1981) from the soma were obtained from visually-identified layer 5 cortical pyramidal cells. An upright microscope (Olympus BX61WI) equipped with oblique illumination and connected to a video camera (PCO CCD Imaging) projected to a LCD monitor aided visualisation of layer 5 cortical pyramidal cells by improving contrast. Patch electrodes were pulled (NARISHIGE PC-10 Puller) with resistances of 5-6 MΩ from thick-walled, filamented borosilicate glass (Harvard Apparatus) and filled with internal solution (~270 mOsm) containing (in mM): 125 CsCl, 10 NaCl, 10 EGTA, 4 Mg-ATP, 0.3 NaGTP and 10 HEPES, pH adjusted to 7.2 with CsOH. Positive pressure was applied and held at 70-90 mbar before inserting the pipette into the bath solution to avoid electrode tip blockage. On approach to the targeted neuron, positive pressure was maintained (50-60 mbar). On formation of a dimple on the somatic membrane, positive pressure was released and a seal formed by applying light negative pressure (< 10 mbar) via gentle suction. Upon formation of a giga-ohm seal, strong and brief suction was employed in order to break in to the cell. Series resistances were 5-25 MΩ. mEPSCs and mIPSCs were recorded at a holding potential of -90 mV and -80 mV respectively. Voltage clamp recordings were made using Multiclamp 700B Amplifier (Molecular Devices), and was low-pass filtered at 2 kHz, before being sampled at 20 kHz using Axograph software (Axograph Scientific) and an ITC-18 interface (Instrutech).

Biocytin labelling. Biocytin (5 mg/ml) was included in the pipette solution for a total of 15 randomly selected layer 5 cortical pyramidal cells from control and $Bbs5^{-/-}$ mice. At the end of the experiment, slices that contained biocytin-marked cells were fixed in 4% paraformaldehyde overnight. Endogenous peroxidases were then blocked using a solution containing 1% H_2O_2 in 10% methanol phosphate-buffered saline. The cells were then permeabilised by 0.4% Triton PBS and labelled with an avidin-biotinylated horseradish peroxidase reaction by incubating them in Avidin/Biotin Complex reagent (Vector Labs, CA) overnight at 4°C . Cells were then

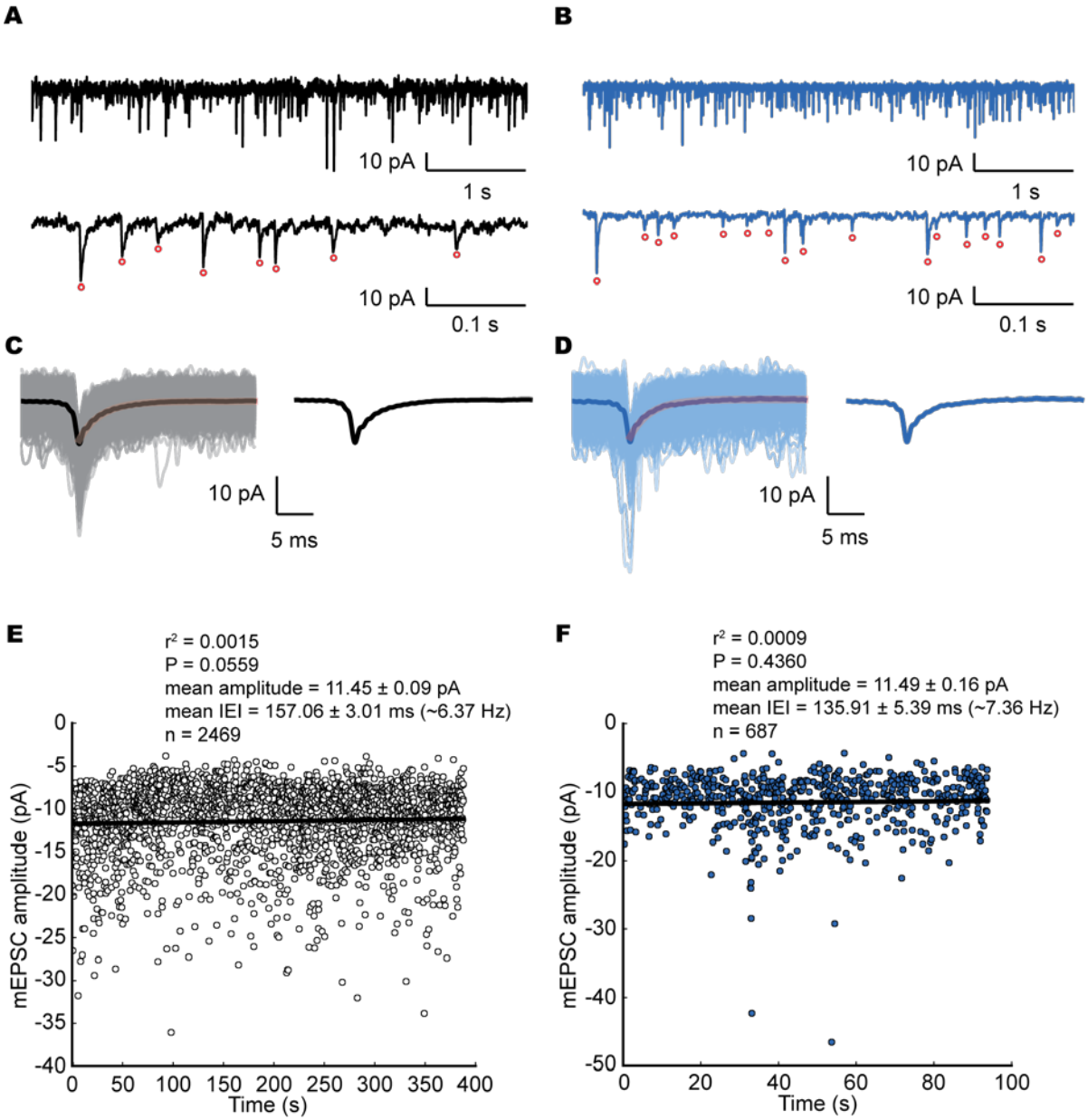

Figure 4. Raw mEPSC data. ***A***, ***B***, Sample traces from whole-cell voltage clamp recordings from layer 5 pyramidal cells at low (top) and high (bottom) magnification, showing inward mEPSCs recorded from wild type (A) and Bbs5$^{-/-}$ (B) cells. (Bottom) Red circles indicate mEPSCs detected by the deconvolution-based algorithm. ***C***, ***D***, Averaged waveforms with (left) and without (right) their superimposed data periods from wild type (***C***) and Bbs5$^{-/-}$ (***D***) example traces. ***E***, ***F***, Stability plots of mEPSC amplitude over time (same cells as in [***C***] and [***D***] respectively). For each plot, a linear regression line is fitted through the data points and its coefficient of determination (r^2), statistical significance (P), mean amplitude, and mean IEI and number of events detected (n) computed.

stained with 0.05% DAB, 0.05% Nickel Ammonium Sulfate and 0.015% H_2O_2 in PBS, and visualised under a light microscope (Olympus BX51). All images were captured using Neurolucida software (http://www.mbfbioscience.com/neurolucida).

Data analysis. Prior to the analysis, a selection process was carried out on all data collected based on a stringent set of criteria. Recordings from cells with high and/or fluctuating holding

current, changing series resistance, and frequent membrane breakdown were discarded. Subsequently, stability plots of mPSC amplitude over time were plotted (Fig. 4*E*, 4*F*, 6*E*, 6*F*). Only recordings that have linear regressions with low coefficients of determination and statistical significance were used. All data were analysed using Stimfit (www.stimfit.org) (Guzman et al., 2014) with custom codes (courtesy of C. Schmidt-Hieber, UCL) developed in Python (www.python.com) based on the Scipy (www.scipy.com), Numpy (www.numpy.com) and MatPlotLib (www.matplotlib.com) modules. mPSC events were detected using a deconvolution-based algorithm (Pernía-Andrade et al., 2012). Data periods surrounding negative peaks were first extracted (muted-coloured waveforms), aligned at the peak and averaged (rich-coloured waveform) (Fig. 4*C*, 4*D*, 6*C*, 6*D*). The peak-aligned average was then fitted with a bi-exponential function (red waveform) which served as a template for event detection (Figure 4*A*, 4*B*, 6*A*, 6*B*). Following event detection, amplitude, frequency, 20-80% rise time, decay time and half-width of mPSCs were extracted. Statistical significance of means and probability distributions were assessed using Mann-Whitney *U* and Kolmogorov-Smirnov test respectively. Significance levels are indicated as *p* values.

Results

Whole-cell patch clamp recordings were obtained from 46 layer 5 cortical pyramidal cells (20 control wild type, 26 Bbs5$^{-/-}$). In order to verify that we were indeed recording from layer 5 cortical pyramidal cells, 15 of those cells were filled with boicytin. Following electrophysiological recordings, biocytin labelling and *post hoc* recovery of cell morphologies confirmed that the recorded cells were indeed layer 5 cortical pyramidal cells (Fig. 3*D*). Gross morphological abnormalities were not found in the Bbs5$^{-/-}$ cells when they were compared to the wild type cells.

No reduction in mPSC frequency and amplitude in Bbs5$^{-/-}$ cortical neurons

The sprouting and retraction of new spines was found to be associated with synapse formation and elimination respectively (Trachtenberg et al., 2002). In investigating the neuronal function of Bbs5, we tested whether the reduction in spine density seen in the two BBS mouse models (S. Christou-Savina and P. Beales, personal communication) could be accompanied by a reduction in synaptic input. Surprisingly, we observed no difference in the frequencies of mEPSCs (control: 6.64 ± 0.79 Hz, n = 14; Bbs5$^{-/-}$: 7.86 ± 1.47 Hz, n = 20; p = 0.493, Mann-Whitney *U* test) (Fig. 5*D*) and mIPSCs (control: 10.78 ± 1.03 Hz, n = 6; Bbs5$^{-/-}$: 11.69 ± 1.16, n = 6; p = 0.236, Mann-Whitney *U* test) (Fig. 7*D*) between control and Bbs5$^{-/-}$ cells. This implies that, should a reduced spine density also be observed in layer 5 cortical pyramidal cells in the Bbs5$^{-/-}$ mouse model, the reduction in spine density was unlikely to be caused by a reduction in the number of synaptic input.

We next looked at the relative amplitudes of mPSCs in control and Bbs5$^{-/-}$ cells. A significant difference between the mean amplitudes of mEPSCs (control: 10.91 ± 0.77 pA, n = 14; Bbs5$^{-/-}$: 11.63 ± 0.75 pA, n = 20; p = 0.226, Mann-Whitney U test) (Fig. 5*A*) and mIPSCs (control: 16.87 ± 1.86 pA, n = 6; Bbs5$^{-/-}$: 18.14 ± 1.90 pA; p = 0.288, Mann-Whitney U test) (Fig. 7*A*) was not detected, suggesting that the size of synaptic inputs was not responsible for the reduction in spine density. In addition, the similar mean frequencies and amplitudes

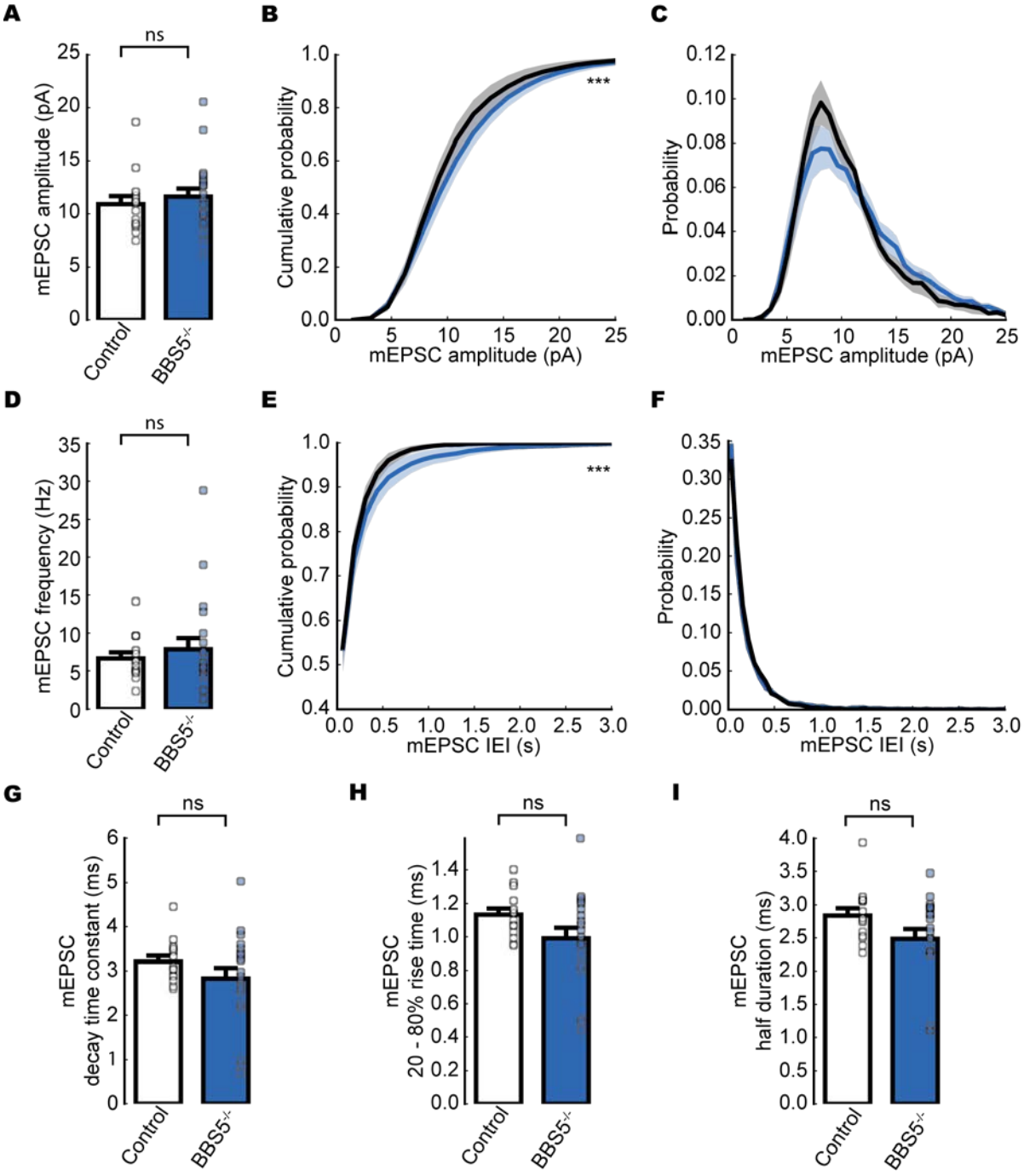

Figure 5. Summary graphs of mEPSC properties. ***A***, Comparison of mean mEPSC amplitudes monitored in wild type and Bbs5$^{-/-}$ cells. ***B***, Cumulative probability histogram of mEPSC amplitudes in wild type (black) and Bbs5$^{-/-}$ (blue) cells. ***C***, Probability plot of mEPSC amplitude in wild type (black) and Bbs5$^{-/-}$ (blue) cells derived from the integration of (***B***). ***D***, Comparison of mean mEPSC frequency monitored in wild type and

Bbs5$^{-/-}$ cells. ***E***, Cumulative probability histogram of mEPSC IEI in wild type (black) and Bbs5$^{-/-}$ (blue) cells. ***F***, Probability plot of mEPSC IEI in wild type (black) and Bbs5$^{-/-}$ (blue) cells derived from the integration of (***E***). ***G***, Comparison of mean mEPSC decay time constant monitored in wild type and Bbs5$^{-/-}$ cells. ***H***, Comparison of mean mEPSC 20-80% rise time monitored in wild type and Bbs5$^{-/-}$ cells. ***I***, Comparison of mean mEPSC half duration monitored in wild type and Bbs5$^{-/-}$ cells. ***A***, ***D***, ***G***–***I***, Data shown are means ± standard error of the mean (SEM); ns p>0.05 as assessed by Mann-Whitney *U* test. Symbols represent means from individual cells. ***B***, ***C***, ***E***, ***F***, Data shown are means (line) ± SEM (shaded area); ***p<0.001 as assessed by Kolmogorov-Smirnov test. ***A***–***I*** Control, n = 14 neurons/3 mice; Bbs5$^{-/-}$, n = 20 neurons/3 mice.

between control and Bbs5$^{-/-}$ cells suggest that the ability to form functional synapses is not defective in Bbs5$^{-/-}$ cells. By extension, should there be an actual reduction in spine density, the non-reduction in the relative synaptic input implies that, at least to a certain extent, synaptogenesis and spinogenesis are mediated by divergent cellular mechanisms. Altogether, the mean amplitude and frequency data hence suggests that Bbs5$^{-/-}$ cells could form functional synapses and that any reduction in spine density is unlikely caused by an altered synaptic function.

Redistribution of the amplitude of synaptic events in Bbs5$^{-/-}$ cortical neurons

In order to compare the distribution of amplitudes of mPSCs between the control and Bbs5$^{-/-}$ mice, we plotted cumulative probability histograms. The mEPSC distributions of both control and Bbs5$^{-/-}$ overlapped to approximately 7.5 pA, beyond which the two distribution deviated (Fig. 5*B*). Specifically, a rightward shift of the Bbs5$^{-/-}$ distribution was observed at larger amplitudes. The difference between the distributions is significant (p = 0.001, Kolmogorov-Smirnov test). This suggested that there are proportionally more larger amplitude events in Bbs5$^{-/-}$ cells. This can be more clearly seen in the amplitude histogram (Fig. 5*C*), which shows proportionally more events that are greater than ~12 pA in amplitude. In line with that, there were proportionally fewer smaller events (i.e. events with amplitudes smaller than ~12 pA). We saw the same trend in the mIPSC amplitude distributions. A significant difference was observed between the distributions of control and Bbs5$^{-/-}$ cells (p = 0.000, Kolmogorov-Smirnov test), with the deviation occurring mostly at the high amplitude end (Fig. 7*B*). Consistently, the amplitude histogram showed a decrease in the number of events with amplitudes smaller than ~15 pA, and a parallel increase in number of bigger events (Fig. 7*C*). Because the mean mEPSC and mIPSC frequencies were similar in control and Bbs5$^{-/-}$ cells (Fig. 5*D*, 7*D*), it is possible that any proportional changes seen in the histograms could reflect absolute changes in numbers. This suggests that there are indeed more larger and less smaller events in Bbs5$^{-/-}$ cells. The increased contribution of larger events is hinted at by the slight but non-significant, increase in mEPSC (Fig. 5*A*) and mIPSC (Fig. 7*A*) mean amplitudes.

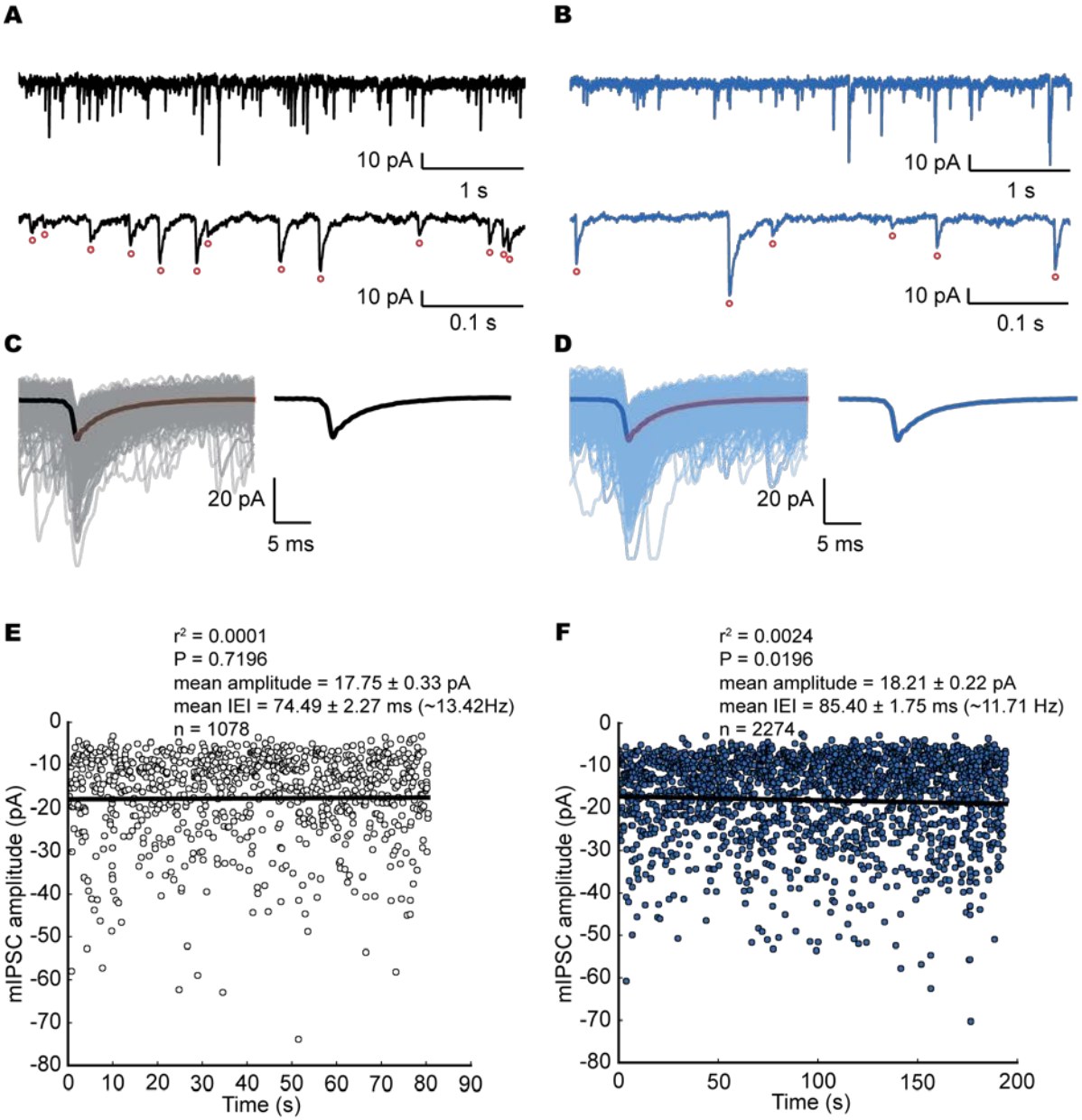

Figure 6. Raw mIPSC data. ***A***, ***B***, Sample traces from whole-cell voltage clamp recordings from layer 5 pyramidal cells at low (top) and high (bottom) magnification, showing inward mIPSCs recorded from wild type (***A***) and Bbs5$^{-/-}$ (***B***) cells. (Bottom) Red circles indicate mIPSCs detected by the deconvolution-based algorithm. ***C***, ***D***, Averaged waveforms with (left) and without (right) their superimposed data periods from wild type (***C***) and Bbs5$^{-/-}$ (***D***) example traces. ***E***, ***F***, Stability plots of mIPSC amplitude over time (same cells as in [***C***] and [***D***] respectively). For each plot, a linear regression line is fitted through the data points and its coefficient of determination (r^2), statistical significance (P), mean amplitude, and mean IEI and number of events detected (n) computed.

A significant difference between the distributions of mEPSC inter-event intervals (IEIs) between control and Bbs5$^{-/-}$ cells was also observed (p = 0.000, Kolmogorov-Smirnov test) (Fig. 5*E*). The distributions of control and Bbs5$^{-/-}$ cells overlapped to approximately 0.3 s, after which point they diverge. However, given that the difference in distribution was only apparent for less than 20% of all IEIs, we think that this difference is not meaningful. This small effect

can also be seen in the IEI histogram, which shows that any difference observed is small (Fig. 5*F*). We however noted that mEPSC IEIs across Bbs5$^{-/-}$ cells are a lot more variable than control cells, as can be seen from an almost two-fold increase in the standard error of the mean (SEM) Bbs5$^{-/-}$ frequency (control: 0.79; Bbs5$^{-/-}$: 1.47) (Fig. 5*D*). Whether this difference is significant and peculiar to the Bbs5$^{-/-}$ phenotype remains to be investigated. In contrast, there was no significant difference between the distributions of mIPSC IEIs in control and Bbs5$^{-/-}$ cells (p = 0.954, Kolmogorov-Smirnov test) (Fig. 7*E*,*F*). Data up to this point suggests that, although no significant difference in the number of functional synapses has been observed, there seems to be a redistribution of the number of small and large events.

Reduced dendritic arborisation length in Bbs5$^{-/-}$ cortical neurons

A major limitation of patch clamping as a point recording technique is that the accuracy of recording the true population response decreases the more extensive the dendrites are. This is due to the passive properties of the dendrite, which causes considerable attenuation and filtering of the synaptic potential as it travels down its site of input towards the soma, where the patch pipette is located in whole-cell recording mode (Williams and Mitchell, 2008). Filtering refers to the slowing of the rise time and the delaying of the peak due to the charging of the membrane capacitance. Voltage attenuation refers to a reduction in the amplitude of the synaptic potential due an outflow of charge through open channels along the membrane. Distal inputs therefore undergo substantial attenuation, fall below the detection threshold and are therefore 'missed'. However, with the underrepresentation of distal inputs aside, this 'bug' presents us with an opportunity to look at the distribution of functional synapses in terms of distance from the soma just by inspecting the amplitude and kinetic properties of mPSCs. Because of the effects discussed above, events proximal to the soma will have a faster rise time and a larger amplitude while distal events tend to have a slower rise time and a smaller amplitude.

In order to approximate the distance of events from the soma, we extracted the kinetic properties of the mPSCs. We found non-significant reductions in the mEPSC decay time constant (control: 3.21 ± 0.13 ms, n = 14; Bbs5$^{-/-}$: 2.83 ± 0.24 ms, n =20; p = 0.151, Mann-Whitney U test), 20-80% rise time (control: 1.13 ± 0.04 ms, n = 14; Bbs5$^{-/-}$: 0.99 ± 0.06 ms, n = 20; p = 0.073, Mann-Whitney U test), and half duration (control: 2.84 ± 0.11 ms, n = 20; Bbs5$^{-/-}$: 2.48 ± 0.15 ms, n = 14; p = 0.095, Mann-Whitney U test) of Bbs5$^{-/-}$ cells. Although not significant, the consistent reduction in all three kinetic parameters is consistent with the idea of reduced electrotonic distance due to a reduction in total dendritic length. This is in agreement with a reduction in total dendritic length seen in Bbs4$^{-/-}$ layer 5 cortical pyramidal cell, Bbs4$^{-/-}$ DGCs, Bbs5$^{-/-}$ DGCs (S. Christou-Savina and P. Beales, personal communication), and DGCs with their primary cilia conditionally ablated (Kumamoto et al., 2012). Similarly, we found a

reduction in all three kinetic parameters extracted from mIPSCs, presumably for the same reason. The reduction in the rise time in Bbs5$^{-/-}$ was not statistically significant (control: 0.91 ± 0.07 ms, n = 6; Bbs5$^{-/-}$: 0.84 ± 0.03 ms, n = 6; p = 0.405, Mann-Whitney U test). In contrast, the reduction in the decay time constant (control: 4.76 ± 0.127 ms, n = 6; Bbs5$^{-/-}$: 4.05 ± 0.25 ms, n = 6; p = 0.033, Mann-Whitney U test) and half duration (control: 3.80 ± 0.16, n = 6; Bbs5$^{-/-}$: 3.18 ± 0.19 ms, n = 6; p = 0.015, Mann-Whitney U test) in Bbs5$^{-/-}$ cells were statistically

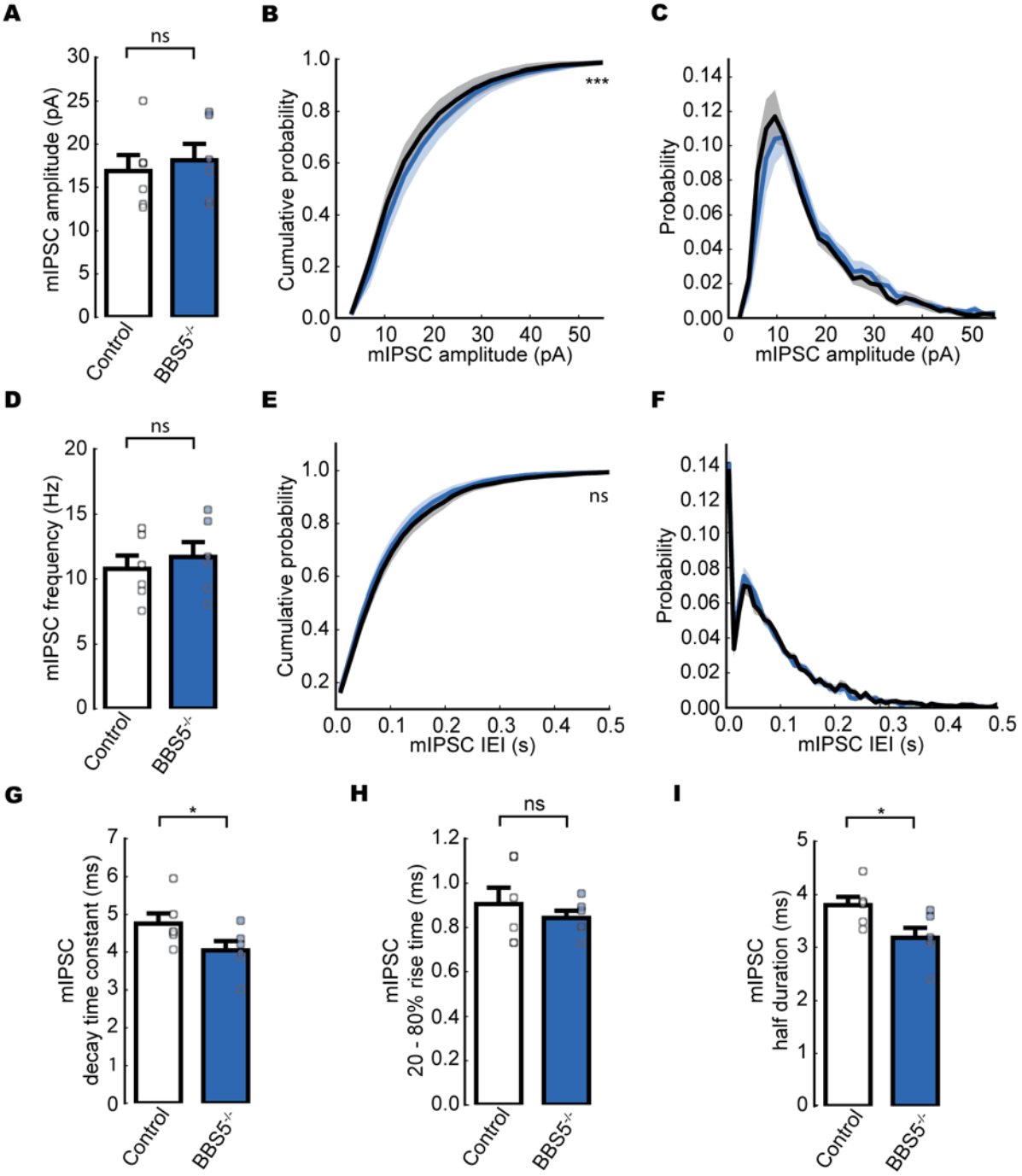

Figure 7. Summary graphs of mIPSC properties. ***A***, Comparison of mean mIPSC amplitudes monitored in wild type and Bbs5$^{-/-}$ cells. ***B***, Cumulative probability histogram of mIPSC amplitudes in wild type (black) and Bbs5$^{-/-}$ (blue) cells. ***C***, Probability plot of mIPSC amplitude in wild type (black) and Bbs5$^{-/-}$ (blue) cells derived from the integration of (***B***). ***D***, Comparison of mean mIPSC frequency monitored in wild type and Bbs5$^{-/-}$ cells.

E, Cumulative probability histogram of mIPSC IEI in wild type (black) and Bbs5$^{-/-}$ (blue) cells. ***F***, Probability plot of mIPSC IEI in wild type (black) and Bbs5$^{-/-}$ (blue) cells derived from the integration of (***E***). ***G***, Comparison of mean mIPSC decay time constant monitored in wild type and Bbs5$^{-/-}$ cells. ***H***, Comparison of mean mIPSC 20-80% rise time monitored in wild type and Bbs5$^{-/-}$ cells. ***I***, Comparison of mean mIPSC half duration monitored in wild type and Bbs5$^{-/-}$ cells. ***A***, ***D***, ***G***–***I***, Data shown are means ± standard error of the mean (SEM); ns p>0.05, *p<0.05 as assessed by Mann-Whitney *U* test. Symbols represent means from individual cells. ***B***, ***C***, ***E***, ***F***, Data shown are means (line) ± SEM (shaded area); ns p>0.05, ***p<0.001 as assessed by Kolmogorov-Smirnov test. ***A***–***I***, Control, n = 6 neurons/1 mouse; Bbs5$^{-/-}$, n = 6 neurons/1 mouse.

significant. Because of dendritic filtering and its extensive effect on the highly-arborized layer 5 cortical pyramidal cells, any differences in channel kinetics would be largely masked. We therefore decided to look at the kinetics data only in terms of extracting distance information of their corresponding events from the soma. Whether Bbs5$^{-/-}$ cells have GABARs with altered subunit composition and channel properties that leads to faster current kinetics remains to be explored.

Synaptic strengthening in individual synapses not apparent in Bbs5$^{-/-}$ cortical neurons

A proportional increase in the number of larger events could imply relative synaptic strengthening of individual synapses due to increased AMPAR or GABAR function and/or re-location of a major portion of the synapses towards perisomatic sites. In order to look at location-specific changes in Bbs5$^{-/-}$ cells in more detail, we plotted amplitude versus rise time of individual events. Because of the concurrent reduction in the size and prolonging of the kinetics of the synaptic potentials due to passive dendritic properties, we expected to see a negative linear relationship between amplitude and rise time. We saw this relationship in most of the cells regardless of their genotype, as judged by their correlation coefficients (*r*) (Fig. 8*A*,*B*,*D*,*E*). Changes to the strength of clusters of synapses at any point along the dendrite can be reflected by changes in the correlation coefficient. With that principle in mind, we posited that the correlation coefficient would provide us with an assay that reflects the nature of changes that might have occurred within the Bbs5$^{-/-}$ cells. We did not find a significant difference in the mean correlation coefficient between control and Bbs5$^{-/-}$ cells for mEPSCs (control: -0.01 ± 0.03, n = 14; Bbs5$^{-/-}$: 0.03 ± 0.03, n = 20; p = 0.237, Mann-Whitney *U* test) (Fig. 8*C*) or mIPSCs (control: 0.11 ± 0.01, n = 6; Bbs5$^{-/-}$: 0.13 ± 0.03, n = 6; p = 0.344, Mann-Whitney *U* test) (Fig. 8*F*), indicating that changes in the strength of specific clusters of synapses situated in particular locations along the somatodendritic axis is unlikely. The redistribution of the sizes of events may hence be better explained by an increase in the number of synapses proximal to the soma and/or a reduction of the number of synapses distal to the soma.

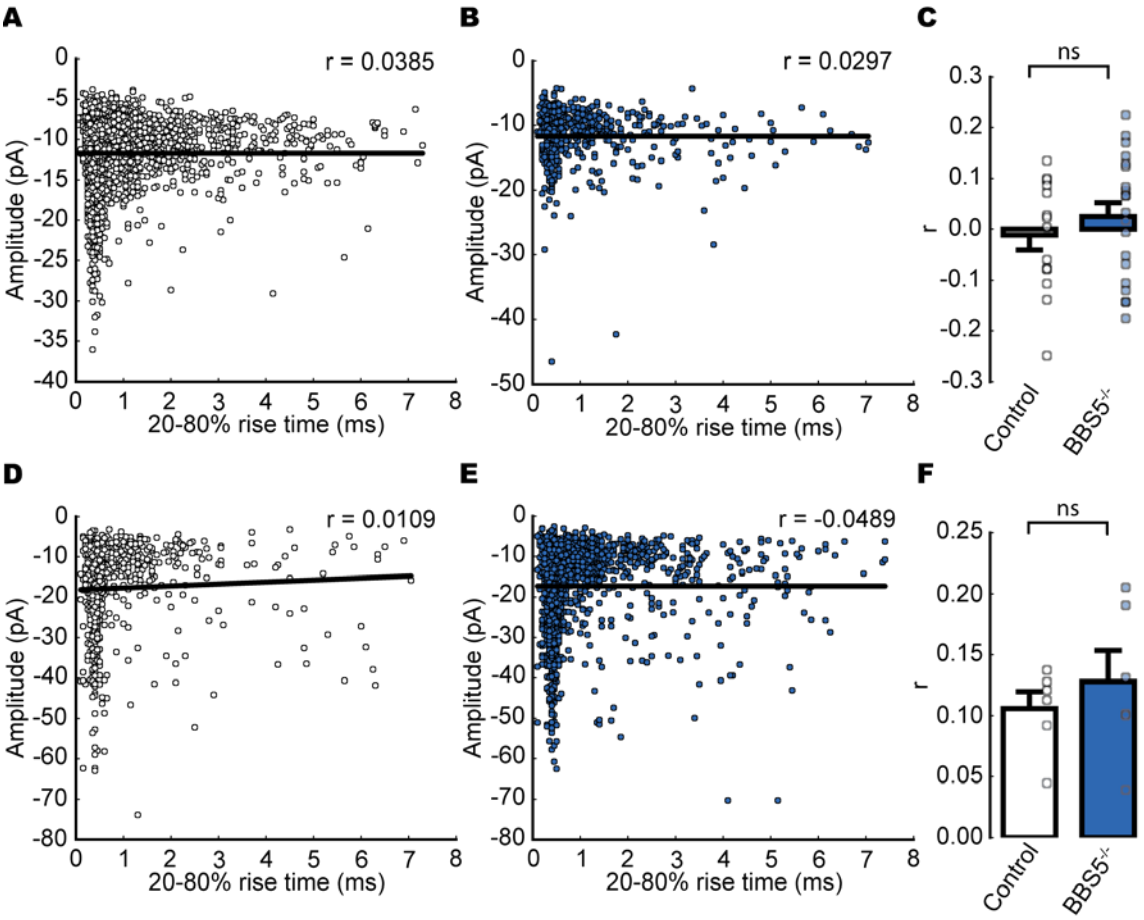

Figure 8. Synaptic strengthening in individual synapses unlikely in Bbs5$^{-/-}$ cortical neurons. ***A***, ***B***, Scatter plots of mEPSC amplitudes versus rise times from example cells (same cells as in Figure 5*C* and 5*D* respectively). A linear regression line is fitted through the data points and its correlation coefficient (*r*) computed. ***C***, Bar graph of mean correlation coefficients derived from scatter plots of mEPSC amplitudes versus rise times for wild type and Bbs5$^{-/-}$ cells (control, n = 14 neurons/3 mice; Bbs5$^{-/-}$, n = 20 neurons/3 mice). ***D***, ***E***, Scatter plots of mIPSC amplitudes versus rise times from example cells (same cells as in Figure 7*C* and 7*D* respectively). A linear regression line is fitted through the data points and its correlation coefficient (*r*) computed. ***F***, Bar graph of mean correlation coefficients derived from scatter plots of mIPSC amplitudes versus rise times for wild type and Bbs5$^{-/-}$ cells (control, n = 6 neurons/1 mouse; Bbs5$^{-/-}$, n = 6 neurons/1 mouse). ***C***, ***F***, Data shown are means ± standard error of the mean (SEM); ns p>0.05, as assessed by Mann-Whitney *U* test. Symbols represent r values of individual cells.

Discussion

Given that learning disabilities are a primary clinical feature of BBS (Beales et al., 1999) and that the forebrain has a known role in cognition, we looked at neuronal circuit formation in the neocortex using electrophysiological approaches. We have shown, using whole-cell patch clamp to record mPSCs in layer 5 cortical pyramidal cells in acute slices, that functional excitatory and inhibitory connectivity is not defective in the neocortex, despite a possible reduction in spine density. We inferred, from the kinetic properties of the mPSCs, that there could be a redistribution of synapses towards the perisomatic regions. This proposal is in line with a possible shortening of the dendritic length in Bbs5$^{-/-}$ cells, as suggested by preliminary

(S. Christou-Savina and P. Beales, personal communication) and kinetics data. Collectively, our results suggest that the impact of Bbs5 deletion on cortical circuit development in the neocortex is more complex than expected.

Redistribution of functional synapses towards perisomatic regions in Bbs5$^{-/-}$ cortical neurons due to possible compensatory mechanisms

Various studies have suggested that alterations in neuronal activity results in modifications in neuronal morphology, in particular the structure of dendrites and spines. For example, two-photon time-lapse imaging of hippocampal CA1 neurons showed that the formation of new spines can be induced by high frequency synaptic stimulation, and does coincide with the induction of long term potentiation (LTP) (Engert and Bonhoeffer, 1999; Maletic-Savatic et al., 1999). In addition, it was shown that LTP-inducing stimuli results in new spines that rapidly contact existing presynaptic boutons and which invariably mature into new synapses 15 to 19 hours after stimulation, suggesting that functional alterations were the basis for structural plasticity (Nägerl et al., 2007). By looking at mPSCs, we therefore wanted to see if we would observe a reduction in synaptic activity in conjunction with a presumed reduction in spine density. We however saw no significant difference between the mean amplitude and frequency of both mEPSCs and mIPSCs recorded. This surprising result has suggested to us two possible explanations.

A significant reduction in overall spine density in Bbs4$^{-/-}$ layer 5 cortical pyramidal cells, Bbs4$^{-/-}$ DGCs and Bbs5$^{-/-}$ DGCs has been observed (S. Christou-Savina and P. Beales, personal communication). The ultrastructure of Bbs5$^{-/-}$ layer 5 cortical pyramidal cells, however, remains to be examined. Therefore it is possible that, contrary to what has been suggested by our preliminary results, there might not be a significant reduction in the overall spine density of Bbs5$^{-/-}$ layer 5 cortical pyramidal cells. This might be consistent with the low reduction in spine density (16%) at a marginal significance level (p = 0.0503) observed in the Bbs5$^{-/-}$ DGCs (control: 1.11 spines/µm, n = 2; Bbs5$^{-/-}$: 0.93 spines/µm, n = 2) (S. Christou-Savina and P. Beales, personal communication). This suggests that, in comparison with Bbs4, Bbs5 has a lesser function in spinogenesis. While every BBS gene is required for BBSome ciliary trafficking (Seo et al., 2011), immunocytochemical analyses showed that the BBS proteins are localised near the centrosome, basal body and cilia, or both, suggesting that they might play dissimilar roles (Ansley et al., 2003). Kim et al. (2004) demonstrated that BBS4 recruitment of PCM1 and associated cargo to the centriolar satellites is required for the proper functioning of the centrosomal microtubule organizing centre (MTOC). Microtubules play an indirect role in spinogenesis. Microtubules lie axially in dendrites and are involved in their growth and maintenance (Hotulainen and Hoogenraad, 2010). Although actin filaments form the main cytoskeleton of dendritic spines (Tada and Sheng, 2006), some of them were found to be

branching off dendritic microtubules (Korobova and Svitkina, 2010). In addition, transient invasion of microtubules into spines have been shown to induce spine head formation and growth (Gu et al., 2008; Jaworski et al., 2009). Therefore, BBS4's role in modulating the MTOC indirectly implicates it in spine formation. In contrast, BBS5 function is more ciliary in nature (Li et al., 2004). For example, the interaction of BBS5 with phosphoinositides is required for ciliogenesis and is thought to underlie the association of the BBSome to the membrane (Nachury et al., 2007). Nevertheless, given that little is known about the interactions and functions of the BBS proteins, the above proposal is speculative until more functional studies are done. Furthermore, definitive evidence of spine density change in the Bbs5$^{-/-}$ mice awaits imaging experiments. In the meantime, we consider other possibilities.

How should we interpret our results if there is indeed a reduction in overall spine density in Bbs5$^{-/-}$ layer 5 cortical pyramidal cells? Considering the fact that synapse number is unchanged (as suggested by unaltered mPSC frequencies; Fig. 5*C*, 7*C*) despite decrease in dendritic arbour length and spine density, two explanations come to mind. Firstly, synaptogenesis might have proceeded as per normal despite "space constraints", independent on dendrito- and spino-genesis. Secondly, there might have been an initial reduction in the number of synapses followed by a compensatory proliferation of 'replacement' synapses. *In vivo* time-lapse imaging followed by serial section electron microscopy analysis will be useful to pry these two possibilities apart, considering the fact that compensatory mechanisms usually take some time to take effect. For example, retinal lesions caused an initial Hebbian reduction in neuronal activity that was followed by a gradual homeostatic return to baseline only in the ensuing 24-48 hours (Keck et al., 2013).

Our results also suggested that there might be a redistribution of synapses to perisomatic sites. This is consistent with the presence of shorter dendritic arbours (S. Christou-Savina and P. Beales, personal communication) and the observed reduction in mPSC kinetic properties. Figure 3*E* (figure courtesy of S. Christou-Savina and P. Beales, Institute of Child Health, London) shows a significant and consistent reduction in spine density across the whole dendritic field in Bbs4$^{-/-}$ cells ($p < 0.05$, ANOVA and post-hoc tests). Regions with less pronounced reductions were not observed, suggesting that any compensatory mechanisms that might have occurred involved the formation of non-spiny synapses. Given that compensatory synapse formation did not induce a parallel increase in the number of spines, we propose that Bbs5$^{-/-}$ layer 5 cortical pyramidal cells exhibit a structural deficit that is independent of synaptic input.

While inhibitory synapses have been found to form on both dendritic spines and shafts, it is well-established that spiny neurons in the brain receive excitatory input exclusively on spines (Shepherd, 2003). Can there be a 'replacement' of excitatory synapses in a neuron with

dysfunctional spine formation? 3D neuronal reconstruction followed by serial electron microscopy of CA1 pyramidal cells showed that the spine-only principle only applies to the distal strata radiatum and oriens dendrites (Megías et al., 2001). Excitatory synapses can be located on dendritic shafts of stratum lacunosum-moleculare, suggesting that spiny neurons are capable of forming non-spiny glutamatergic inputs. Moreover, it has been shown that ~30% of the synapses found in layer 1 of the rat somatosensory cortex is formed on shafts (Vaughan and Peters, 1973; Trachtenberg et al., 2002).

We however note that the electrophysiological characterisation, although necessary, is insufficient to come to a definite conclusion particularly on synapse number. Characterisation of the distribution of synapses via serial section electron microscopy will therefore be needed to see if the functional alterations observed here is corroborated by structural changes (e.g. membrane thickening and other evidence of functional synapses). In addition, immunogold labelling or immunostaining of receptors might be helpful in looking at receptor-specific changes in localisation, although electrophysiological evidence suggest an indiscriminate redistribution of both AMPAR and GABAR towards perisomatic sites (Fig. 5*C*, 7*C*).

The role of primary ciliogenesis in the development of neuronal signalling and connectivity

In addition to the known role of primary cilia in specialised sensory cells (see above), there is increasing evidence that primary cilia are critical for the development of the vertebrate nervous system (Guemez-Gamboa et al., 2014). Several lines of inquiry have suggested that the primary cilium is required for the proper formation of dendrites – the failure of which is associated with abnormal synaptic function and defective synaptic integration. Disruption of primary cilia assembly in DGCs, either by the expression of dominant-negative Kif3a (dnKif3a) or the knocking down of Ift88 – both essential for IFT – led to an ablation of primary cilia and a substantially shorter dendritic arbour length, although differences in the number and complexity of dendritic branches were not observed (Kumamoto et al., 2012). The reduction in dendritic arbour length was also shown to be associated with a reduction in the frequency, but not the amplitude, of spontaneous EPSC, suggesting that a functional primary cilium is not necessary for the formation of normal synapses, but might affect its number. This is expected because a shortened dendritic arbour length would naturally limit the chance of an incoming axonal projection to make contact. Overexpression of ciliary GPCRs 5-hydroxytryptamine receptor 6 (5HT6) and Shekel Somatostatin receptor type 3 (SSTR3) in developing neocortical neurons induces the formation of abnormally long and branched cilia, and significantly reduces the complexity of dendritic arborisation to the extent of that induced in dnKif3a-positive neurons (Guadiana et al., 2013). This importantly showed that aberrant cilia assembly in either direction leads to abnormal dendritic morphogenesis.

Our present and preliminary results add to and might possibly confound the findings above. Knockdown of BBS5$^{-/-}$ in retinal pigmented epithelium (RPE) cells has been shown to cause the most dramatic reduction in ciliation of the first 12 BBS genes (BBS1-12) (Nachury et al., 2007; Loktev et al., 2008). Our preliminary results show that Bbs5$^{-/-}$ reduces both dendritic length and spine density in DGCs (S. Christou-Savina and P. Beales, personal communication). Together, these findings reinforce the idea that the primary cilium is critical for proper dendrite formation. On the other hand, it has been shown that the knockdown of BBS4 in culture and Bbs4 in mice does not significantly reduce the ciliation of RPE cells and kidney epithelial cells respectively (Mykytyn et al., 2004; Loktev et al., 2008). Although not investigated in neurons, evidence suggests that BBS4 might not be essential for ciliogenesis. Despite this, a reduction in dendritic length and spine density was demonstrated in Bbs4$^{-/-}$ layer 5 cortical pyramidal cells and DGCs (S. Christou-Savina and P. Beales, personal communication). Hence, contrary to prevailing evidence, this implies either that the primary cilium per se might not be essential for proper dendrite formation and/or disruption of a divergent dendritogenesis mechanism in Bbs4$^{-/-}$ cells.

A role for BBS5 in learning and memory?

BBS is known for its high neurological involvement (Valente et al., 2014). Psychological testing suggested that BBS patients had deficits in IQ and social skills (Brinckman et al., 2013). Recent findings also hinted at the importance of Bbs genes for learning and memory as disrupting cortical and hippocampal ciliogenesis in mice was shown to disrupt aversive memory and novel object recognition (Berbari et al., 2014). In addition, type 3 adenylyl cyclase, a GPCR exclusively expressed in the primary cilium, was found to be crucial for short-term memory and contextual fear conditioning (Wang et al., 2011). Given that we found no deficits of synaptic function in the neocortex in Bbs5$^{-/-}$ mice, we suggest that BBS5 defects in the neocortex have a lesser role in learning impairments in BBS patients. Instead, BBS5 defects might have a greater impact on adult neurogenesis in the hippocampus (Bennouna-Greene et al., 2011). Regardless, the role of Bbs5$^{-/-}$ in animal learning is unexplored and needs to be behaviourally tested before conclusions can be drawn from synaptic data.

In conclusion, we find that Bbs5 plays a nuanced role in altering functional connectivity in the mouse neocortex. Whether this is corroborated by structural and behavioural data awaits further investigation.

References

Ansley S, Badano J, Blacque O, Hill J (2003) Basal body dysfunction is a likely cause of pleiotropic Bardet–Biedl syndrome. Nature 425 Available at: http://www.nature.com/nature/journal/v425/n6958/abs/nature02030.html [Accessed November 2, 2014].

Beales P, Elcioglu N, Woolf A, Parker D, Flinter F (1999) New criteria for improved diagnosis of Bardet-Biedl syndrome: results of a population survey. :437–446 Available at: http://discovery.ucl.ac.uk/106231/.

Bennouna-Greene V, Kremer S, Stoetzel C, Christmann D, Schuster C, Durand M, Verloes a, Sigaudy S, Holder-Espinasse M, Godet J, Brandt C, Marion V, Danion a, Dietemann J-L, Dollfus H (2011) Hippocampal dysgenesis and variable neuropsychiatric phenotypes in patients with Bardet-Biedl syndrome underline complex CNS impact of primary cilia. Clin Genet 80:523–531 Available at: http://www.ncbi.nlm.nih.gov/pubmed/21517826 [Accessed November 2, 2014].

Berbari NF, Malarkey EB, Yazdi SMZR, McNair AD, Kippe JM, Croyle MJ, Kraft TW, Yoder BK (2014) Hippocampal and cortical primary cilia are required for aversive memory in mice. PLoS One 9:e106576 Available at: http://www.pubmedcentral.nih.gov/articlerender.fcgi?artid=4153651&tool=pmcentrez&rendertype=abstract [Accessed November 2, 2014].

Brinckman DD, Keppler-Noreuil KM, Blumhorst C, Biesecker LG, Sapp JC, Johnston JJ, Wiggs E a (2013) Cognitive, sensory, and psychosocial characteristics in patients with Bardet-Biedl syndrome. Am J Med Genet A 161A:2964–2971 Available at: http://www.ncbi.nlm.nih.gov/pubmed/24194441 [Accessed November 2, 2014].

Christensen ST, Voss JW, Teilmann SC, Lambert IH (2005) High expression of the taurine transporter TauT in primary cilia of NIH3T3 fibroblasts. Cell Biol Int 29:347–351.

Engert F, Bonhoeffer T (1999) Dendritic spine changes associated with hippocampal long-term synaptic plasticity. Nature 399:66–70.

Forsythe E, Beales PL (2012) Bardet–Biedl syndrome. Eur J Hum Genet:8–13.

Forsythe E, Beales PL (2014) Bardet-Biedl Syndrome. In: GeneReviews® [Internet] (Pagon R, Adam M, Ardinger H, eds). Seattle (WA): University of Washington, Seattle. Available at: http://www.ncbi.nlm.nih.gov/books/NBK1363/ [Accessed March 21, 2015].

Goetz SC, Anderson K V (2010) The primary cilium: a signalling centre during vertebrate development. Nat Rev Genet 11:331–344 Available at: http://dx.doi.org/10.1038/nrg2774.

Gu J, Firestein BL, Zheng JQ (2008) Microtubules in dendritic spine development. J Neurosci 28:12120–12124.

Guadiana SM, Semple-Rowland S, Daroszewski D, Madorsky I, Breunig JJ, Mykytyn K, Sarkisian MR (2013) Arborization of dendrites by developing neocortical neurons is dependent on primary cilia and type 3 adenylyl cyclase. J Neurosci 33:2626–2638 Available at: http://www.ncbi.nlm.nih.gov/pubmed/23392690.

Guemez-Gamboa A, Coufal NG, Gleeson JG (2014) Primary Cilia in the Developing and Mature Brain. Neuron 82:511–521 Available at: http://dx.doi.org/10.1016/j.neuron.2014.04.024.

Guzman SJ, Schlögl A, Schmidt-Hieber C (2014) Stimfit: quantifying electrophysiological data with Python. Front Neuroinform 8:16 Available at: http://www.pubmedcentral.nih.gov/articlerender.fcgi?artid=3931263&tool=pmcentrez&rendertype=abstract.

Hamill O, Marty A, Neher E, Sakmann B, Sigworth F (1981) Improved patch-clamp techniques for high-resolution current recording from cells and cell-free membrane patches. Pflügers Arch:85–100 Available at: http://link.springer.com/article/10.1007/BF00656997 [Accessed July 11, 2014].

Haycraft CJ, Banizs B, Aydin-Son Y, Zhang Q, Michaud EJ, Yoder BK (2005) Gli2 and Gli3 localize to cilia and require the intraflagellar transport protein polaris for processing and function. PLoS Genet 1:e53.

Higginbotham H, Guo J, Yokota Y, Umberger NL, Su C-Y, Li J, Verma N, Hirt J, Ghukasyan V, Caspary T, Anton ES (2013) Arl13b-regulated cilia activities are essential for polarized radial glial scaffold formation. Nat Neurosci 16:1000–1007 Available at: http://www.pubmedcentral.nih.gov/articlerender.fcgi?artid=3866024&tool=pmcentrez&rendertype=abstract [Accessed November 2, 2014].

Hotulainen P, Hoogenraad CC (2010) Actin in dendritic spines: Connecting dynamics to function. J Cell Biol 189:619–629.

Huangfu D, Anderson K V (2005) Cilia and Hedgehog responsiveness in the mouse. Proc Natl Acad Sci U S A 102:11325–11330.

Insinna C, Besharse JC (2008) Intraflagellar transport and the sensory outer segment of vertebrate photoreceptors. Dev Dyn 237:1982–1992.

Jaworski J, Kapitein LC, Gouveia SM, Dortland BR, Wulf PS, Grigoriev I, Camera P, Spangler S a., Di Stefano P, Demmers J, Krugers H, Defilippi P, Akhmanova A, Hoogenraad CC (2009) Dynamic Microtubules Regulate Dendritic Spine Morphology and Synaptic Plasticity. Neuron 61:85–100 Available at: http://dx.doi.org/10.1016/j.neuron.2008.11.013.

Keck T, Keller GB, Jacobsen RI, Eysel UT, Bonhoeffer T, Hübener M (2013) Synaptic scaling and homeostatic plasticity in the mouse visual cortex in vivo. Neuron 80:327–334.

Kim JC, Badano JL, Sibold S, Esmail M a, Hill J, Hoskins BE, Leitch CC, Venner K, Ansley SJ, Ross AJ, Leroux MR, Katsanis N, Beales PL (2004) The Bardet-Biedl protein BBS4 targets cargo to the pericentriolar region and is required for microtubule anchoring and cell cycle progression. Nat Genet 36:462–470.

Korobova F, Svitkina T (2010) Molecular architecture of synaptic actin cytoskeleton in hippocampal neurons reveals a mechanism of dendritic spine morphogenesis. Mol Biol Cell 21:165–176.

Kuhara A (2012) Temperature Sensing by an Olfactory. Sci Technol 803:803–808.

Kumamoto N, Gu Y, Wang J, Janoschka S, Takemaru K-I, Levine J, Ge S (2012) A role for primary cilia in glutamatergic synaptic integration of adult-born neurons. Nat Neurosci 15:399–405, S1 Available at: http://www.pubmedcentral.nih.gov/articlerender.fcgi?artid=3288565&tool=pmcentrez&rendertype=abstract [Accessed November 2, 2014].

Lancaster M a, Schroth J, Gleeson JG (2011) Subcellular spatial regulation of canonical Wnt signalling at the primary cilium. Nat Cell Biol 13:700–707 Available at: http://dx.doi.org/10.1038/ncb2259.

Li JB et al. (2004) Comparative genomics identifies a flagellar and basal body proteome that includes the BBS5 human disease gene. Cell 117:541–552.

Li Z, Sheng M (2003) Some assembly required: the development of neuronal synapses. Nat Rev Mol Cell Biol 4:833–841.

Loktev A V., Zhang Q, Beck JS, Searby CC, Scheetz TE, Bazan JF, Slusarski DC, Sheffield VC, Jackson PK, Nachury M V. (2008) A BBSome Subunit Links Ciliogenesis, Microtubule Stability, and Acetylation. Dev Cell 15:854–865 Available at: http://dx.doi.org/10.1016/j.devcel.2008.11.001.

Louvi A, Grove E a. (2011) Cilia in the CNS: The quiet organelle claims center stage. Neuron 69:1046–1060 Available at: http://dx.doi.org/10.1016/j.neuron.2011.03.002.

Maletic-Savatic M, Malinow R, Svoboda K (1999) Rapid dendritic morphogenesis in CA1 hippocampal dendrites induced by synaptic activity. Science 283:1923–1927.

Markov NT, Ercsey-Ravasz M, Van Essen DC, Knoblauch K, Toroczkai Z, Kennedy H (2013) Cortical High-Density Counterstream Architectures. Science (80-) 342:1238406–1238406 Available at: http://www.sciencemag.org/cgi/doi/10.1126/science.1238406.

Megías M, Emri Z, Freund TF, Gulyás AI (2001) Total number and distribution of inhibitory and excitatory synapses on hippocampal CA1 pyramidal cells. Neuroscience 102:527–540 Available at: http://www.ncbi.nlm.nih.gov/pubmed/11226691 [Accessed December 24, 2014].

Moorman SJ, Shorr AZ (2008) The primary cilium as a gravitational force transducer and a regulator of transcriptional noise. Dev Dyn 237:1955–1959.

Mykytyn K, Mullins RF, Andrews M, Chiang AP, Swiderski RE, Yang B, Braun T, Casavant T, Stone EM, Sheffield VC (2004) Bardet-Biedl syndrome type 4 (BBS4)-null mice implicate Bbs4 in flagella formation but not global cilia assembly. Proc Natl Acad Sci U S A 101:8664–8669.

Nachury M V., Loktev A V., Zhang Q, Westlake CJ, Peränen J, Merdes A, Slusarski DC, Scheller RH, Bazan JF, Sheffield VC, Jackson PK (2007) A Core Complex of BBS Proteins Cooperates with the GTPase Rab8 to Promote Ciliary Membrane Biogenesis. Cell 129:1201–1213.

Nägerl UV, Köstinger G, Anderson JC, Martin K a C, Bonhoeffer T (2007) Protracted synaptogenesis after activity-dependent spinogenesis in hippocampal neurons. J Neurosci 27:8149–8156.

Pernía-Andrade AJ, Goswami SP, Stickler Y, Fröbe U, Schlögl A, Jonas P (2012) A deconvolution-based method with high sensitivity and temporal resolution for detection of spontaneous synaptic currents in vitro and in vivo. Biophys J 103:1429–1439.

Satir P, Pedersen LB, Christensen ST (2010) The primary cilium at a glance. J Cell Sci 123:499–503.

Seo S, Zhang Q, Bugge K, Breslow DK, Searby CC, Nachury M V., Sheffield VC (2011) A novel protein LZTFL1 regulates ciliary trafficking of the BBSome and smoothened. PLoS Genet 7.

Shepherd GMG (2003) The Synaptic Organization of the Brain (Shepherd GM, ed)., 5th ed. Oxford University Press. Available at: http://www.amazon.com/Synaptic-Organization-Brain-Gordon-Shepherd/dp/019515956X [Accessed March 22, 2015].

Szymanska K, Johnson C a (2012) The transition zone: an essential functional compartment of cilia. Cilia 1:10 Available at: Cilia.

Tada T, Sheng M (2006) Molecular mechanisms of dendritic spine morphogenesis. Curr Opin Neurobiol 16:95–101.

Tobin JL, Beales PL (2007) Bardet-Biedl syndrome: beyond the cilium. Pediatr Nephrol 22:926–936 Available at: http://www.ncbi.nlm.nih.gov/pubmed/17357787 [Accessed November 2, 2014].

Trachtenberg JT, Chen BE, Knott GW, Feng G, Sanes JR, Welker E, Svoboda K (2002) Long-term in vivo imaging of experience-dependent synaptic plasticity in adult cortex. Nature 420:788–794.

Valente EM, Rosti RO, Gibbs E, Gleeson JG (2014) Primary cilia in neurodevelopmental disorders. Nat Rev Neurol 10:27–36 Available at: http://www.pubmedcentral.nih.gov/articlerender.fcgi?artid=3989897&tool=pmcentrez&rendertype=abstract.

Vaughan DW, Peters a (1973) A three dimensional study of layer I of the rat parietal cortex. J Comp Neurol 149:355–370.

Waites CL, Craig AM, Garner CC (2005) Mechanisms of vertebrate synaptogenesis. Annu Rev Neurosci 28:251–274.

Wallingford JB, Mitchell B (2011) Strange as it may seem: The many links between Wnt signaling, planar cell polarity, and cilia. Genes Dev 25:201–213.

Wang Z, Phan T, Storm DR (2011) The type 3 adenylyl cyclase is required for novel object learning and extinction of contextual memory: role of cAMP signaling in primary cilia. J Neurosci 31:5557–5561.

Williams SR, Mitchell SJ (2008) Direct measurement of somatic voltage clamp errors in central neurons. Nat Neurosci 11:790–798.